Residual trapping of supercritical CO_2 in oil-wet sandstone

Taufiq Rahman, [1*] Maxim Lebedev, [2] Ahmed Barifcani, [3] Stefan Iglauer, [1]

[1] *Department of Petroleum Engineering, Curtin University, 26 Dick Perry Avenue, 6151 Kensington, Australia*

[2] *Department of Exploration Geophysics, Curtin University, 26 Dick Perry Avenue, 6151 Kensington, Australia[2] Department of Chemical Engineering*

[3]*Department of Chemical Engineering, Curtin University, 26 Dick Perry Avenue, 6151 Kensington, Australia*

[*]corresponding author (taufiq.rahman@curtin.edu.au)

Abstract

Residual trapping, a key CO_2 geo-storage mechanism during the first decades of a sequestration project, immobilizes micrometre sized CO_2 bubbles in the pore network of the rock. This mechanism has been proven to work in clean sandstones and carbonates; however, this mechanism has not been proven for the economically most important storage sites into which CO_2 will be initially injected at industrial scale, namely oil reservoirs. The key difference is that oil reservoirs are typically oil-wet or intermediate-wet, and it is clear that associated pore-scale capillary forces are different. And this difference in capillary forces clearly reduces the capillary trapping capacity (residual trapping) as we demonstrate here. For an oil-wet rock (water contact angle θ = 130°) residual CO_2 saturation $S_{CO2,r}$ (≈ 8%) was approximately halved when compared

to a strongly water-wet rock ($\theta = 0°$; $S_{CO2,r} \approx 15\%$). Consequently, residual trapping is less efficient in oil-wet reservoirs.

Keywords:

CO_2 geo-sequestration; Residual trapping; Storage capacity; Wettability; Oil-wet; Oil reservoir

1. Introduction

Carbon geo-sequestration has been identified as a feasible technology to mitigate global warming [1-3]. Technically, CO_2 is captured from large emitters (e.g. coal-fired power plants), and injected deep underground into geological formations for storage. However, although CO_2 is in a dense supercritical state at reservoir conditions (below 800m depth), it migrates upwards as it has a lower density than the resident formation brine. One key mechanism, which prevents the CO_2 from leaking back to the surface is residual trapping, where the CO_2 plume is split into many micrometre sized bubbles which are immobilized by capillary forces in the pore network of the rock [4-8]. Pore-scale residual trapping has been proven to work in clean sandstone [7] and carbonate [9,10]. However, this mechanism has not been proven for oil-wet rock, despite its key importance as initial industrial scale CO_2 storage projects are very likely to occur in oil reservoirs [11]; and these oil reservoirs are typically oil-wet [12]. The significance of oil reservoirs for carbon storage is high, as sequestration can be directly combined with CO_2 driven enhanced oil recovery [13-15]; furthermore, depleted oil reservoirs already have required infrastructure in place [16], and they are typically well characterised in

terms of seismic surveys, which significantly aids (reservoir scale) CO_2 flow monitoring [17].

We thus imaged initial and residual CO_2 in an oil-wet rock at typical storage conditions with an x-ray micro-computed tomograph (μCT), and we demonstrate that the residual trapping capacity is significantly reduced in oil-wet rock at (high pressure) storage conditions.

2. Experimental Procedure

2.1 Simulating subsurface conditions

A sandstone oil reservoir at a depth of approximately 1000m was simulated (10MPa pore pressure, 318K temperature). For this, a clean homogeneous sandstone (Bentheimer) was selected to represent storage rock. Small core plugs (5mm diameter and 10mm length) were drilled and used for the experiments. Porosity was 22%, permeability 1800mD, and the rock consisted of 99wt% quartz, 0.7wt% kaolinite, and 0.3wt% rutile.

This rock was completely water-wet at ambient conditions (0° water contact angle in air), note that at higher pressures quartz is less water-wet [18-20]. To mimic an oil reservoir the wettability of the rock was altered by immersing the plug into silane (Dodecyltriethoxysilane, 99.9mol% purity, from Sigma-Aldrich) under vacuum (so that the plug was fully saturated with the silane) and ageing the plug for 4 weeks at ambient conditions [21]. This process rendered the plug strongly oil-wet (130° water contact angle at ambient conditions in air).

2.2 Imaging scCO$_2$ at the pore-scale with μCT

The oil-wet core plug was mounted into a high pressure μCT cell [7], vacuumed and fully saturated with doped "dead" brine (7wt% NaI in deionized water; note that NaI is required for CT contrast). Subsequently 15 MPa confining pressure was applied, and pore pressure was raised to 10MPa. All flow lines and fluids were isothermally heated to 318K. These conditions approximately correspond to a storage depth of 1000m, see above. The dead brine was then displaced with >40 pore volumes (PV) of "live" brine (live brine is brine thermodynamically equilibrated with CO_2; [22]). Then 40PV of supercritical (sc) CO_2 were injected at a flow rate of 0.1 mL/min, which corresponded to a capillary number of 6×10^{-8}, and the core plug was imaged in 3D at a resolution of $(3.4\mu m)^3$ with an Xradia VersaXRM μCT instrument. Finally live brine (40PV) was injected at a flow rate of 0.1mL/min, which corresponded to a capillary number of 1.7×10^{-6}, and the sample was μCT imaged again. This experiment was repeated again, and the results were reproducible. The μCT images were filtered with a 3D non-local means algorithm [23] and segmented with a watershed algorithm [24]. Petrophysical properties were then measured on the images, see below. For comparison, the same experiment was conducted again with a water-wet Bentheimer plug (0° water contact angle, see above).

3. Results and Discussion

3.1 Visualization, cluster morphologies and initial and residual CO_2 saturations

Initial and residual CO_2 saturations of the oil-wet and water-wet plugs are visualized in Figure 1. Initial CO_2 saturations ($S_{CO2,i}$) were approximately the same (~50%), but the residual saturation ($S_{CO2,r}$) in the oil-wet plug was significantly lower (≈8 %) than in the

water-wet plug ($S_{CO2,r} \approx 15\%$), Table 1. Precisely, the $S_{CO2,r}$ measured for the water-wet plug was 14.9%, consistent with independent measurements ([5,6,7,9,25,26]; note that $S_{CO2,r}$ varies to some degree as it is also a function of porosity [27] and pore body-pore throat aspect ratio [28,29]); and CO_2 was located mainly in larger pores, although in some cases it also spread into relatively small pores. This indicates weakly water-wet conditions, consistent with 2D micromodel [30,31] and contact angle [18-20,32-39] measurements.

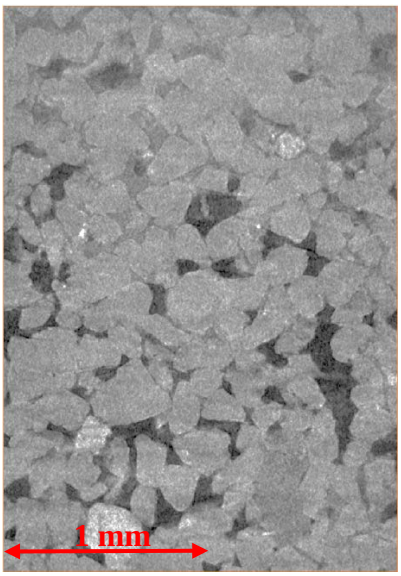

(a)

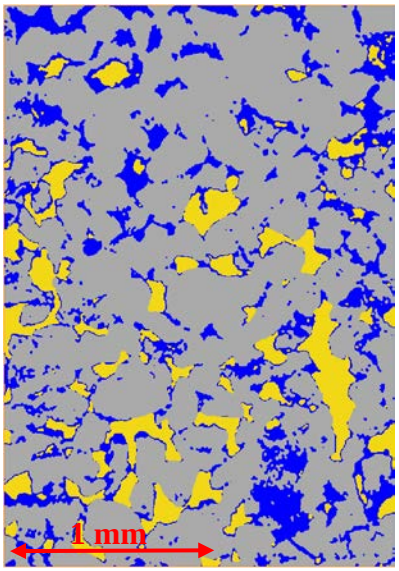

(b)

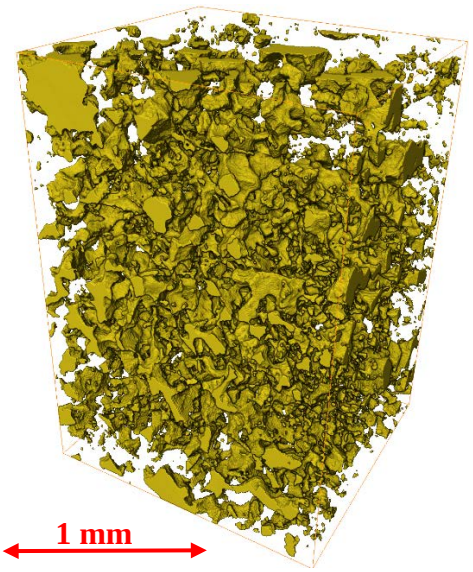

(c)

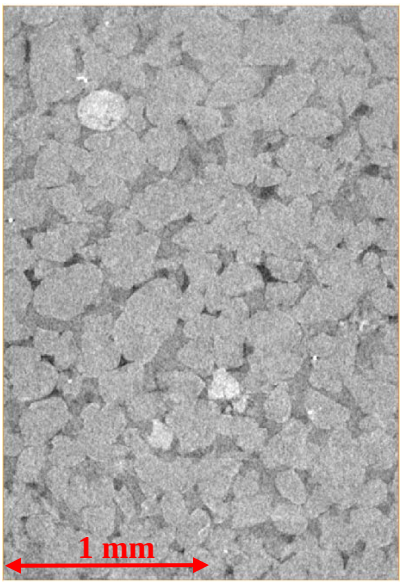

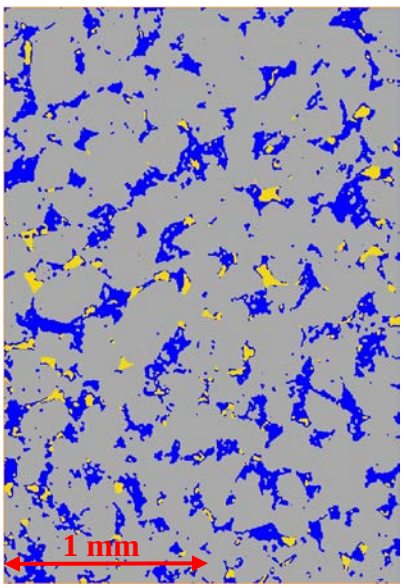

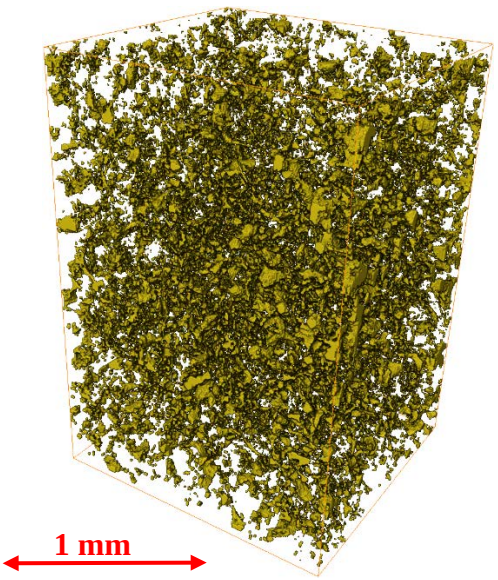

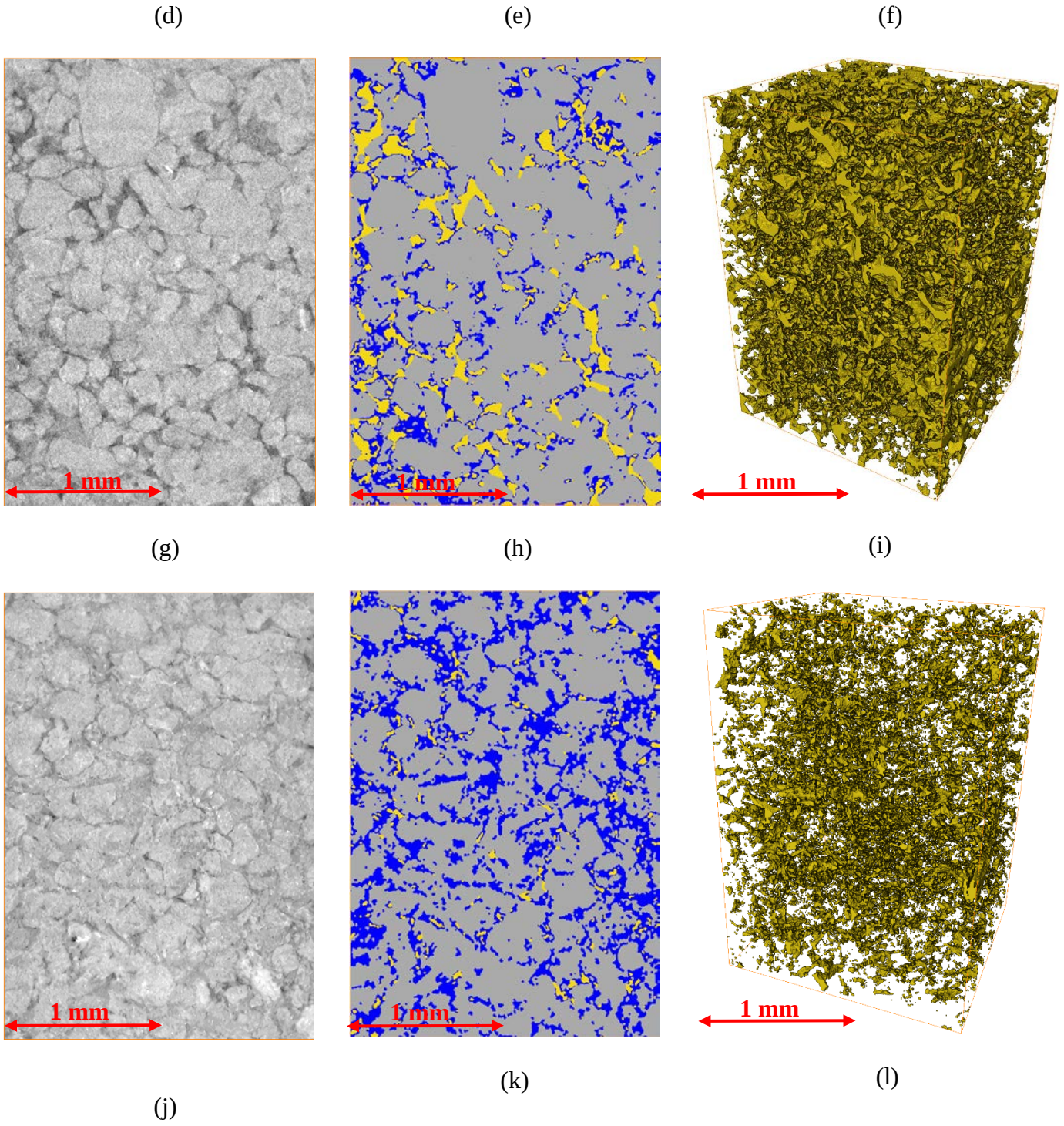

Figure 1. µCT image of Bentheimer sandstone at 10MPa pore pressure and 318K: (a) water-wet initial CO_2 saturation, raw image; (b) water-wet initial CO_2 saturation, segmented image; (c) CO_2 clusters in 3D for the water-wet initial CO_2 saturation, a

105 volume of 3mm^3 is shown; (d) water-wet residual CO_2 saturation, raw image; (e) water-
106 wet residual CO_2 saturation, segmented image; (f) CO_2 clusters in 3D for the water-wet
107 residual CO_2 saturation, a volume of 3mm^3 is shown; (g) oil-wet initial CO_2 saturation,
108 raw image; (h) oil-wet initial CO_2 saturation, segmented image; (i) CO_2 clusters in 3D
109 for the oil-wet initial CO_2 saturation, a volume of 3mm^3 is shown; (j) oil-wet residual
110 CO_2 saturation, raw image; (k) oil-wet residual CO_2 saturation, segmented image; (l)
111 CO_2 clusters in 3D for the oil-wet residual CO_2 saturation, a volume of 3mm^3 is shown.
112 CO_2 is black/dark grey, brine is grey and sandstone is light grey; in the segmented
113 images CO_2 is yellow, brine is blue and rock is grey.
114
115 **Table 1.** Initial and residual CO_2 saturations in water-wet and oil-wet Bentheimer
116 sandstone at 318K and 10MPa pore pressure.

Wettability state	Contact angle [°][a]	Initial CO_2 saturation [%]	Residual CO_2 saturation [%]
Water-wet	0	50.6	14.9
Oil-wet	130	49.2	8.7

117 [a]water contact angle in air at ambient conditions.
118
119 The fact that $S_{CO2,r}$ was significantly lower in the oil-wet plug (8.7%, i.e. ~40% less
120 CO_2 was trapped in this scenario) is consistent with measurements in an oil-wet plastic
121 bead pack [40], where a substantial reduction of residual scCO_2 was observed when
122 compared to a water-wet analogue. Furthermore, CO_2 was frequently located in smaller
123 pores and adjacent to rock surfaces, which indicates intermediate- or CO_2-wet
124 behaviour. Such wetting behaviour was also observed in 2D micromodels [30] and
125 contact angle measurements [41-45].

The morphology of the CO_2 clusters in the water-wet plug was also different than in the oil-wet plug (Figure 2): while the CO_2 clusters in case of the initial CO_2 saturation state in the water-wet plug were bulky and essentially mimicked the pore space geometry, the corresponding residual CO_2 clusters thinned out considerably and had a somewhat fractal-like shape. Compare this with observations for an oil-water system in a completely water-wet sandstone ([46]; which is known to be strongly water-wet, also at reservoir conditions [47]); here the initial and residual clusters mimicked the pore geometry. We conclude that the more fractal-like shape for the residual CO_2 clusters is caused by a shift towards weakly water-wet conditions (CO_2-brine-quartz is weakly water-wet at reservoir conditions, (e.g.[20]). The initial CO_2 clusters in the oil-wet plug were already thinner, more "skeleton-like", than their water-wet counterparts, and the associated residual CO_2 clusters were flat and sheet-like (Figure 2d). This is somewhat similar to what has been observed for an oil-water system in an intermediate-wet sandstone [48], where sheet-like residual oil clusters were observed. This indicates that the oil-wet plug showed intermediate-wet or CO_2-wet behaviour, consistent with 2D micromodel and contact angle measurements, see above.

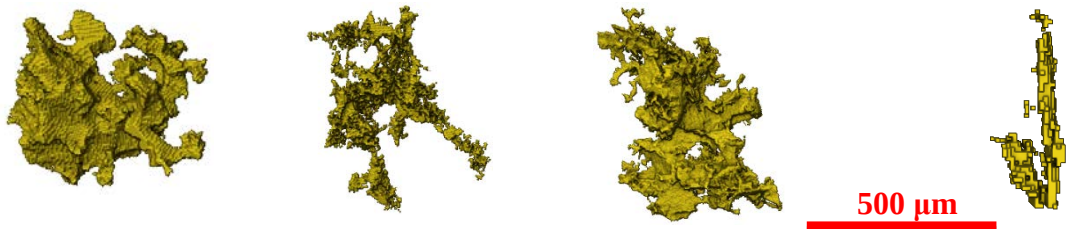

Figure 2. Morphologies and volumes of the largest initial and residual CO_2 clusters in Bentheimer sandstone at 318K and 10MPa pore pressure: (a) water-wet initial CO_2

saturation (volume = 27.7 x 10^6 μm^3), (b) water-wet residual CO_2 saturation (volume = 5.39 x 10^6 μm^3), (c) oil-wet initial CO_2 saturation (volume = 18.4 x 10^6 μm^3), (d) oil-wet residual CO_2 saturation (volume = 3.03 x 10^6 μm^3).

3.2. CO_2 cluster statistics

3.2.1 CO_2 cluster size distributions

CO_2 cluster size distributions were analysed for all scenarios (oil-wet, water-wet, residual, initial), they are plotted in Figure 3. As in other experiments of this type [e.g. 7,9,10,46,48-52] power-law correlations were observed ($N \propto V^{-\tau}$, where N is the count number of clusters of size V, and τ is a fitting exponent), Table 2.

Table 2. Statistical parameters associated with the initial and residual CO_2 clusters for oil-wet and water-wet sandstone (Bentheimer, 318K, 10MPa pore pressure).

Plug state		τ	p
Water-wet	Initial CO_2	1	0.79
	Residual CO_2	1.6	0.85
Oil-wet	Initial CO_2	1	0.83
	Residual CO_2	1.9	0.85

This essentially means that, for each scenario, a large number of small clusters was observed, and only few large clusters. As expected the largest CO_2 clusters at initial CO_2 saturation state (V_{max} = 28 x 10^{-6} μm^3 for the water-wet rock and V_{max} = 18 x 10^{-6} μm^3 for the oil-wet rock) were significantly reduced by waterflooding (V_{max} = 5 x 10^{-6} μm^3 for the water-wet rock and V_{max} = 3 x 10^{-6} μm^3 for the oil-wet rock). Furthermore,

the largest clusters always spanned almost the entire observed volume, which may imply that waterflooding (especially in oil-wet reservoirs) reduces the efficiency of structural trapping as the height of the CO_2 plume may not be affected while the CO_2 saturation in the bulk rock is reduced.

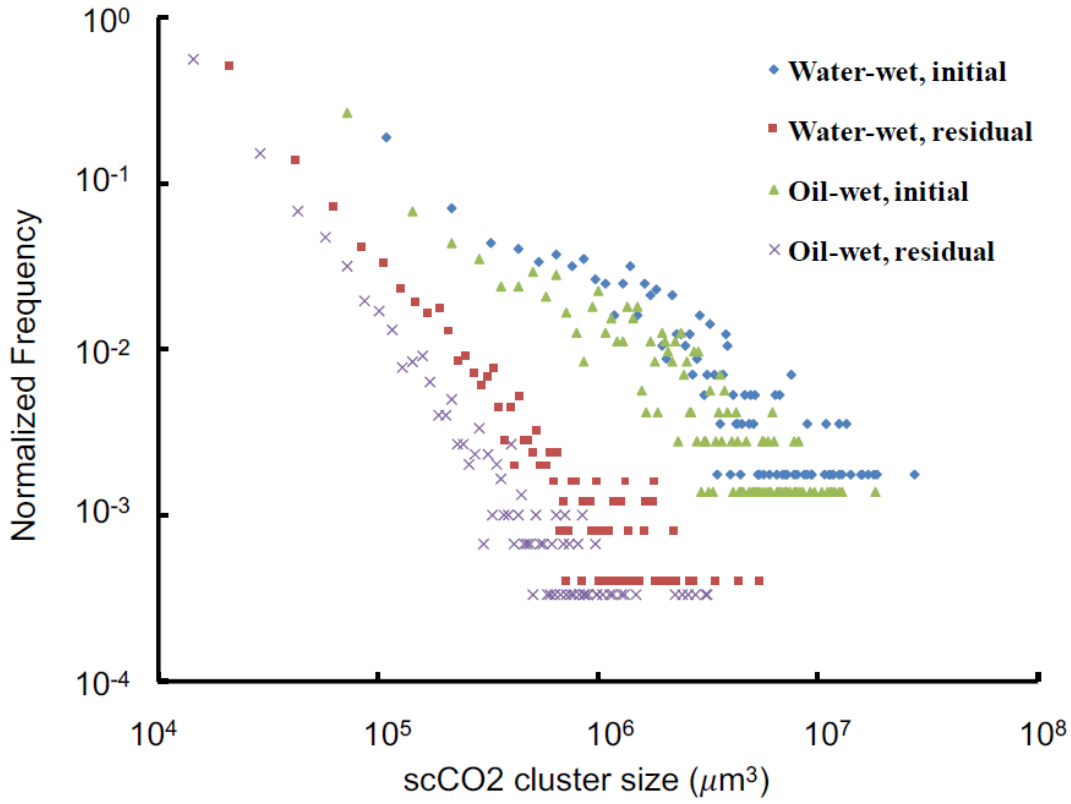

Figure 3. Initial and residual CO_2 droplet size distributions measured in water-wet and oil-wet Bentheimer sandstone at 318K and 10MPa pore pressure.

With respect to the scaling exponent τ; τ was significantly increased by waterflooding; this effect is caused by snap-off of many small CO_2 droplets [53]. Interestingly, τ increased more in the oil-wet plug, an effect which must be caused by the wettability (as all other parameters were constant, see methods section above). Mechanistically, CO_2

180 can enter small pores in the oil-wet plug (due to the lower capillary entry pressure
181 constraint [54]; as oil-wet surfaces are more CO_2-wet, cp. review paper by [37]), and
182 these CO_2 volumes in the smaller pore channels may also snap-off, leading to additional
183 small clusters (= larger τ).
184
185 **3.2.2 CO_2-water interfacial areas**
186 Subsequently, surface areas *A* for each CO_2 cluster were measured and plotted against
187 their volumes *V*, cp. Figure 4. From the graph again a power-law relation is evident ($A \sim V^{-p}$);
188 and as with all other measurements of this kind [28,49,55], *p* was always ~0.8.
189

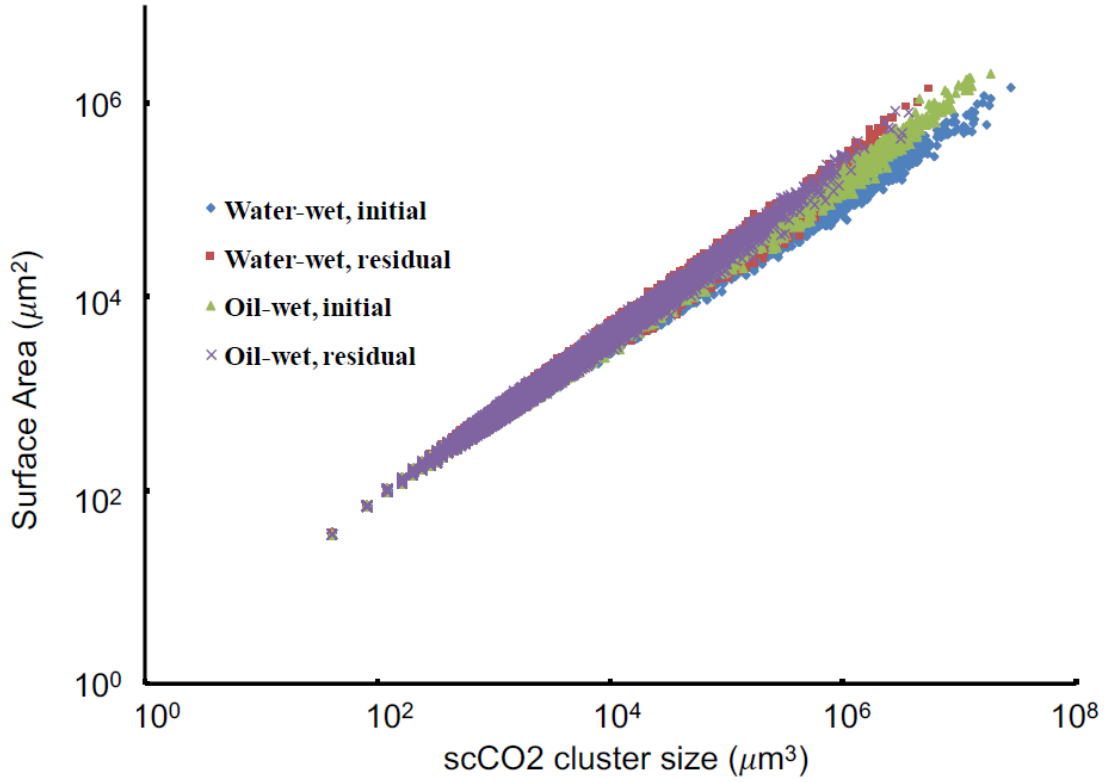

190
191
192 **Figure 4.** CO_2 droplet surface areas plotted against their volumes for various
193 conditions, at 318K and 10MPa pore pressure.

194 In this context it is interesting to note that the power-law exponents measured (τ and p)
195 are significantly lower than predicted by percolation theory (which predicts τ = 2.189
196 and p ≈1;[56,57]). We conclude that simple percolation models will not deliver accurate
197 and reliable predictions, as already evident in Georgiadis et al.'s work [50].
198
199 **3.2.3 Capillary pressure distributions**
200 Finally, we measured curvatures (*C*) of each cluster, and calculated associated capillary
201 pressures (p_c) for each CO_2 bubble and water droplet ($p_c = \gamma C$; Figure 5) assuming a
202 water-CO_2 interfacial tension γ of 40mN/m [58,59].
203
204 The capillary pressure distributions were roughly bell-tower shaped, and always showed
205 a narrow and high peak around zero capillary pressure, consistent with data reported for
206 oil-water systems [60]. Nominally the capillary pressures ranged from ~-0.4 MPa to +
207 0.3MPa in case of CO_2, and from -0.6MPa to +0.6MPa in case of water (the water
208 distributions were slightly stretched to the left, Figure 5b).

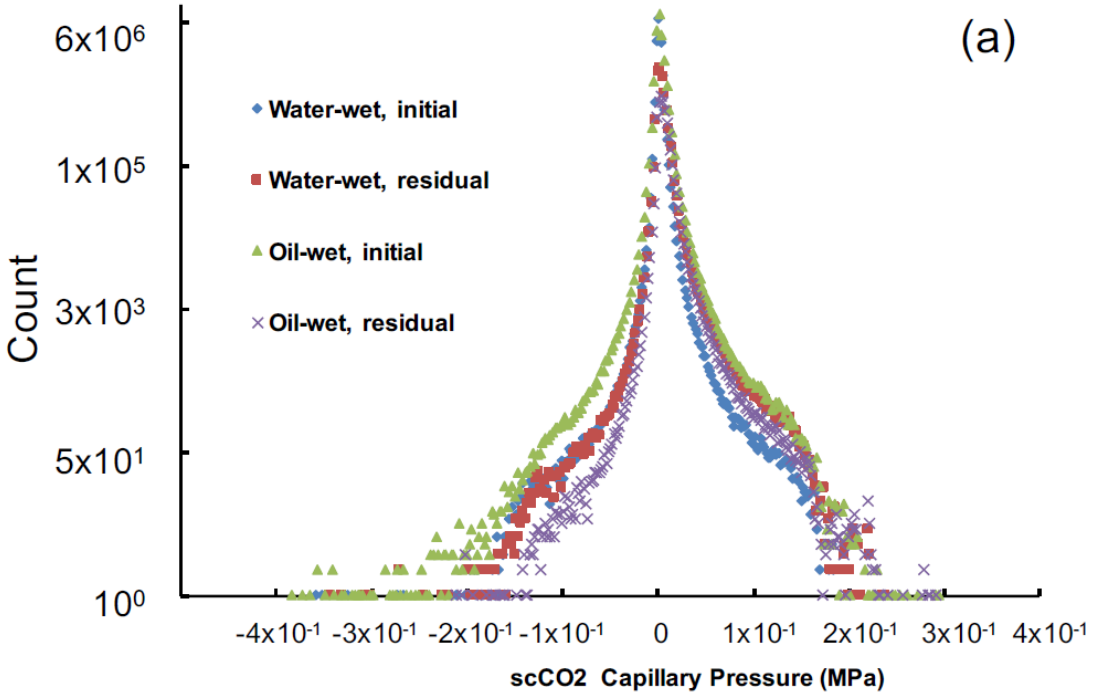

209

210

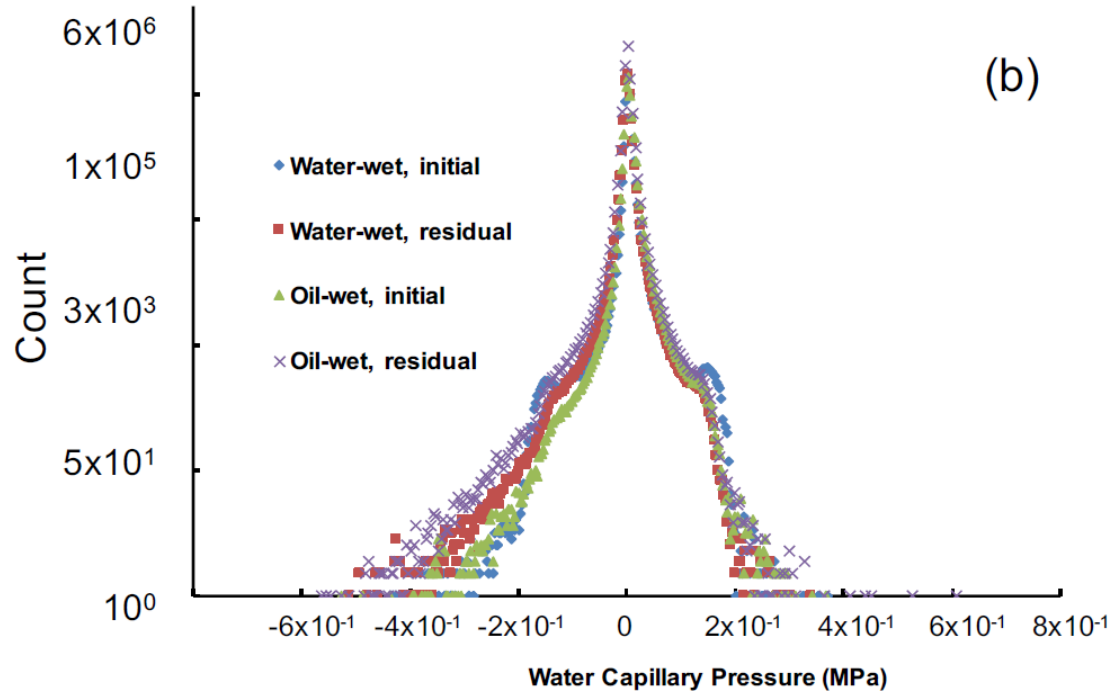

211

212

213 **Figure 5.** CO_2 (a) and water (b) droplet capillary pressures measured in water-wet and

214 oil-wet Bentheimer sandstone at 318K and 10MPa pore pressure.

4. Conclusions and Implications

We demonstrated that residual CO_2 saturations ($S_{CO2,r}$) in oil-wet sandstone are dramatically lower than in equivalent water-wet sandstone ($S_{CO2,r}$ = 8.7% versus 14.9%). This is consistent with data reported for a plastic bead pack [40], and indicates that oil-wet rock is intermediate-wet or CO_2-wet at reservoir conditions; a phenomenon which was also observed in independent contact angle measurements [41-45]. This shift in CO_2-wettability also significantly influenced CO_2 cluster morphologies and residual cluster size distributions: flatter and more sheet-like clusters and more small CO_2 bubbles were observed in the oil-wet sample.

We conclude that, importantly, residual trapping is less efficient in oil reservoirs than in deep saline aquifers.

Acknowledgements

The measurements were performed using the μCT system courtesy of the National Geosequestration Laboratory (NGL) of Australia. The NGL is a collaboration between Curtin University, CSIRO, and the University of Western Australia established to conduct and deploy critical research and development to enable commercial-scale carbon storage options. Funding for this facility was provided by the Australian Federal Government.

References

[1] Lackner, K.S. (2003) Climate change. A guide to CO_2 sequestration, *Science*, 300, 1677-1678, doi:10.1126/science.1079033.

240 [2] Intergovernmental Panel on Climate Change (IPCC) (2005) *IPCC special report*
241 *on carbon dioxide capture and storage*, prepared by Working Group III of the
242 Intergovernmental Panel on Climate Change, Cambridge University Press.
243 [3] Orr, F.M. (2009) Onshore geologic storage of CO_2, *Science*, 325, 1656-1658,
244 doi:10.1126/science.1175677.
245 [4] Juanes, R., Spiteri, E.J., Orr, F.M., and M. J. Blunt (2006) Impact of relative
246 permeability hysteresis on geological CO_2 storage, *Water Resour. Res.*, 42, 1–13,
247 doi: 10.1029/2005WR004806.
248 [5] Suekane, T., Nobuso, T., Hirai, S., and M. Kiyota (2008) Geological storage of
249 carbon dioxide by residual gas and solubility trapping, *Int. J. Greenhouse Gas*
250 *Control*, 2(1), 58-64.
251 [6] Pentland, C. H., El-Maghraby, R., Iglauer, S., and M. J. Blunt (2011)
252 Measurements of the capillary trapping of super-critical carbon dioxide in Berea
253 sandstone, *Geophys. Res. Lett.*, 38, L06401, doi:10.1029/2011GL046683.
254 [7] Iglauer, S., A. Paluszny, C. H. Pentland, and M. J. Blunt (2011a) Residual CO_2
255 imaged with X-ray micro-tomography, *Geophysical Research Letters*, 38, 21,
256 L21403, doi: 10.1029/2011GL049680.
257 [8] Krevor, S. C. M., R. Pini, L. Zuo, and S. M. Benson (2012) Relative
258 permeability and trapping of CO_2 and water in sandstone rocks at reservoir
259 conditions, *Water Resour. Res.*, 48, W02532, doi:10.1029/2011WR010859.
260 [9] Andrew, M., Bijeljic, B., and M.J. Blunt (2013) Pore-scale imaging of
261 geological carbon dioxide storage under in situ conditions; *Geophysical Research*
262 *Letters* 40 (15), 3915-3918, doi: 10.1002/grl.50771.
263 [10] Andrew, M., Bijeljic, B., and M.J. Blunt (2014) Pore-scale imaging of trapped
264 supercritical carbon dioxide in sandstones and carbonates, International Journal of
265 Greenhouse Gas Control 22, 1-14.
266 [11] Firoozabadi, A., and P. Cheng (2010) Prospects for subsurface CO_2
267 sequestration, *AIChE Journal*, 56(6), 1398-1405.
268 [12] Cantucci, B., Montegrossi, G., Vaselli, O., Tassi, F., Quattrocchi, F., and
269 Perkins, E.H. (2009) Geochemical modelling of CO_2 storage in deep reservoirs: The
270 Weyburn Project (Canada) case study, *Chemical Geology*, 265, 181-197.

[13] Lake L. W. "Enhanced Oil Recovery." SPE ATCE. Training Courses. Florence, Italy: Society of Petroleum Engineers, September 23, 2010.

[14] Emberley S., Hutcheon, I., Shevalier, M., Durocher, K., Mayer, B., Gunter W.D., Perkins E.H. (2005) Monitoring of fluid-rock interaction and CO_2 storage through produced fluid sampling at the Weyburn CO_2-injection enhanced oil recovery site, Saskatchewan, *Applied Geochemistry*, 20, 1131-1157.

[15] Cuiec, L.E (1991) Evaluation of reservoir wettability and its effect on oil recovery. In: Interfacial Phenomena in Petroleum Recovery (ed.: N.R. Morrow). New York: Marcel Dekker.

[16] Cook, P.J (Ed) (2014) *Geologically Storing Carbon: Learning from the Otway Project Experience*. CSIRO Publishing , Melbourne. IBSN 9781486302321.

[17] Gurevich, B., Pevzner, R., Urosevic, M., Kepic, A., Shulakova, V., Caspari, E., Lebedev, M (2014) "2D and 3D seismic investigations for Stages 1 and 2C. " In *Geologically Storing Carbon: Learning from the Otway Project Experience.* Editor: Cook P.J. CSIRO Publishing, Melbourne. 155-196, IBSN 9781486302321.

[18] Chiquet, P., Broseta, D. and S. Thibeau (2007) Wettability alteration of caprock minerals by carbon dioxide, *Geofluids*, 7, 112–122.

[19] Broseta, D., Tonnet, N., Shah, V. (2012) Are rocks still water-wet in the presence of dense CO_2 or H_2S?, *Geofluids*, 12, 280-294.

[20] Al-Yaseri, A. Z., Lebedev, M., Barifcani, A., S. Iglauer (2015) Receding and advancing CO_2-brine-quartz contact angles as a function of pressure, temperature, surface roughness, salt type and salinity, J. Chem. Thermodynamics, S0021-9614(15)00255-4, doi:10.1016/j.jct.2015.07.031.

[21] Al-Anssari, S., Barifcani, A., Wang, S., Lebedev, M., and S. Iglauer (2016) Wettability alteration of oil-wet carbonate by silica nanofluid, *Journal of Colloid and Interface Science*, 461, 435-442.

[22] El-Maghraby, R., Pentland, C.H., Iglauer, S., and M.J. Blunt (2012) A fast method to equilibrate carbon dioxide with brine at high pressure and elevated temperature including solubility measurements, *Journal of Supercritical Fluids*, 62, 55-59.

[23] Buades, A., Coll, B., and J.M. Morel (2005) A non-local algorithm for image denoising, *Proc. Computer Vision and Pattern Recognition*, 2, 60-65.

303 [24] Schlüter, S., Sheppard, A., Brown, K., and D. Wildenschild (2014) Image
304 processing of multiphase images obtained via microtomography: a review. *Water*
305 *Resources Research*. WR015256. 3615-3639, doi: 10.1002/2014WR015256.
306 [25] Krevor, S. C. M., Blunt, M.J., Benson, S.M., Pentland, C.H., Reynolds, C., Al-
307 Menhali, A., and B. Niu (2015) Capillary trapping for carbon dioxide storage – from
308 pore scale physics to field scale implications, *International Journal of Greenhouse*
309 *Gas Control*, 40, 221-237.
310 [26] Akbarabadi, M., and M. Piri (2013) Relative permeability hysteresis and
311 capillary trapping characteristics of supercritical CO_2/brine systems: An
312 experimental study at reservoir conditions, *Adv. Water Resour.*, 52, 190–206.
313 [27] Iglauer, S., Wülling, W., Pentland, C.H., Al-Mansoori, S., and M.J. Blunt
314 (2011b) Capillary trapping capacities of consolidated rocks and sands, *SPE Journal*,
315 16, 4, 778-783.
316 [28] Pentland, C.H., Iglauer, S., Gharbi, O., Okada, K., and T. Suekane (2012) The
317 Influence of Pore Space Geometry on the Entrapment of Carbon Dioxide by
318 Capillary Forces, SPE 158516, *SPE Asia Pacific Oil and Gas Conference and*
319 *Exhibition*, Perth, Australia.
320 [29] Wardlaw, N.C., and L. Yu (1988) Fluid topology, pore size and aspect ratio
321 during imbibition, *Transport in Porous Media*, 3(1), 17-34.
322 [30] Chalbaud, C., Robin, M., Lombard, J.-M., Bertin, H., and P. Egermann (2010)
323 Brine/CO_2 interfacial properties and effects on CO_2 storage in deep saline aquifers,
324 *Oil & Gas Science and Technology*, 65(4), 541-555.
325 [31] Kim, Y., J. Wan, T. J. Kneafsey, and T. K. Tokunaga (2012) Dewetting of silica
326 surfaces upon reactions with supercritical CO_2 and brine: Pore scale studies in
327 micromodels, *Environ. Sci. Technol.*, 46(7), 4228–4235.
328 [32] Farokhpoor, R., Bjørkvik, B.J.A., Lindeberg, E., and O. Torsæter (2013)
329 Wettability behaviour of CO_2 at storage conditions, *International Journal of*
330 *Greenhouse Gas Control*, 12, 18-25.
331 [33] Saraji, S., Goual, L., Piri, M., and H. Plancher (2013) Wettability of supercritical
332 carbon dioxide/water/quartz systems: Simultaneous measurement of contact angle
333 and interfacial tension at reservoir conditions, *Langmuir*, 29, 6856–6866.

334 [34] Saraji, S., Piri, M., and L. Goual (2014) The effects of SO_2 contamination, brine
335 salinity, pressure, and temperature on dynamic contact angles and interfacial tension
336 of CO_2/brine/quartz systems, *Int. J. Greenhouse Gas Control*, 28, 147–155.
337 [35] Kaveh, N. S., Rudolph, E.S.J., van Hemert, P., Rossen, W.R., and K. H. Wolf
338 (2014) Wettability evaluation of a CO_2/water/Bentheimer sandstone system:
339 Contact angle, dissolution, and bubble size, *Energy & Fuels*, 28(6), 4002-4020.
340 [36] Sarmadivaleh, M., A.Z. Al-Yaseri, and S. Iglauer (2015) Influence of
341 temperature and pressure on quartz-water-CO_2 contact angle and CO_2-water
342 interfacial tension, *Journal of Colloid and Interface Science*, 441, 59-64,
343 doi:10.1016/j.jcis.2014.11.010.
344 [37] Iglauer, S., C.H. Pentland, and A. Busch (2015a) CO_2-wettability of seal and
345 reservoir rocks and the implications for carbon geo-sequestration, *Water Resources*
346 *Research*, 51, 1, 729-774, WR015553, doi: 10.1002/wrcr.21095.
347 [38] Iglauer, S., Al-Yaseri, A.Z., Rezaee, R., and M. Lebedev (2015b) CO_2-
348 wettability of caprocks: Implications for structural storage capacity and containment
349 security, *Geophysical Research Letters*, in press, doi: 10.1002/2015GL065787.
350 [39] Al-Yaseri, A. Z., Sarmadivaleh, M., Saeedi, A., Lebedev, M., Barifcani, A., S.
351 Iglauer (2015) N_2+CO_2+NaCl brine interfacial tensions and contact angles on
352 quartz at CO_2 storage site conditions in the Gippsland basin, Victoria/Australia,
353 *Journal of Petroleum Science and Engineering*, S0920-4105(15)00027-3, doi:
354 10.1016/j.petrol.2015.01.026.
355 [40] Chaudhary, K., Bayani Cardenas, M., Wolfe, W.W., Maisano, J.A., Ketcham,
356 R.A., and P.C. Bennett (2013) Pore-scale trapping of supercritical CO_2 role of
357 grain wettability and shape, *Geophysical Research Letters*, 40, 15, 3878-3882, doi:
358 10.1002/grl.50658.
359 [41] Ameri, A., Kaveh, N. S., Rudolph, E. S. J., Wolf, K. H., Farajzadeh, R., and J.
360 Bruining, (2013) Investigation on interfacial interactions among crude oil–brine–
361 sandstone rock–CO_2 by contact angle measurements. *Energy & Fuels*, 27(2), 1015-
362 1025.
363 [42] Dickson, J.L., Gupta, G., Horozov, T.S., Binks, B.P. and K.P. Johnston, K.P.
364 (2006) Wetting Phenomena at the CO_2/Water/Glass Interface, *Langmuir*, 22(5),
365 2161-2170.

366 [43] Espinoza, D.N., and J.C. Santamarina (2010) W ater-CO_2-mineral systems:
367 Interfacial tension, contact angle, and diffusion – Implications to CO_2 geological
368 storage, *Water Resour Res*, 46, 7, W0753, doi:10.1029/2009WR008634.
369 [44] Yang, D., Gu, Y., and P. Tontiwachwuthikul (2007) Wettability determination
370 of the reservoir brine− reservoir rock system with dissolution of CO_2 at high
371 pressures and elevated temperatures, *Energy & Fuels*, 22(1), 504-509.
372 [45] Yang, D., Gu, Y., and P. Tontiwachwuthikul (2008) Wettability Determination
373 of the Crude Oil− Reservoir Brine− Reservoir Rock System with Dissolution of
374 CO_2 at High Pressures and Elevated Temperatures, *Energy & Fuels*, 22(4), 2362-
375 2371.
376 [46] Iglauer, S., S. Favretto, G. Spinelli, G. Schena, and M. J. Blunt (2010) X-ray
377 tomography measurements of power-law cluster size distributions for the
378 nonwetting phase in sandstones, *Physical Review E*, 82, 056315.
379 [47] Xie, X., and N.R. Morrow (1998) Wetting of Quartz by Oleic/Aqueous Liquids
380 and Adsorption from Crude Oil, *Colloids and Surfaces*, 138, 97-108.
381 [48] Iglauer, S., M. A. Fernø, P. Shearing, and M. J. Blunt (2012) Comparison of
382 residual oil cluster size distribution, morphology and saturation in oil-wet and water-
383 wet sandstone, *Journal of Colloid and Interface Science*, 375, 1, 187–192.
384 [49] Iglauer, S., A. Paluszny, and M. Blunt (2013) Simultaneous oil recovery and
385 residual gas storage: a pore-level analysis using in-situ x-ray micro-tomography.
386 *Fuel.* 1, 1-11.
387 [50] Georgiadis, A., Berg, S., Makurat, A., Maitland, G, Ott, H. (2013) Pore-scale
388 micro-computed tomography imaging: non-wetting-phase cluster-size distribution
389 during drainage and imbibition, *Physical Review E*, 88, 033002.
390 [51] Geistlinger H, Mohammadian S, Schlüter S, Vogel HJ (2014) Quantification of c
391 apillary trapping of gasclusters using X- ray microtomography. *Water Resource*
392 *Research*, 50, 4514–29.
393 [52] Geistlinger, H., Mohammadian, S. (2015) Capillary trapping mechanism in
394 strongly water-wet systems: comparison between experiment and percolation
395 theory, *Advances in Water Resources*, 79, 35-50.
396 [53] Roof, J.G. (1970) Snap-off of oil droplets in water-wet pores, *SPE Journal*,
397 10(1), 85-90.

[54] Oren, P.E., Billiote, J., and W.V. Pinczewski (1992) Mobilization of waterflood residual oil by gas injection for water-wet conditions, *SPE Form Eval.* 7, 70-78.

[55] Karpyn, Z.T., Piri, M., and G. Singh (2010) Experimental investigation of trapped oil clusters in a water-wet bead pack using x-ray microtomography, *Water Resources Research*, 46, 4, W04510, doi: 10.1029/2008WR007539.

[56] Stauffer, D. (1979) Scaling theory of percolation clusters. *Phys Rep*. 54, 1-74.

[57] Lorenz, C.D., and R.M. Ziff (1998) Precise determination of the bond percolation thresholds and finite-size scaling corrections for the sc, fcc, and bcc lattices, *Physical Review E*, 57,230-237.

[58] Li, X., E. Boek, G.C. Maitland, and J.P.M. Trusler (2012) Interfacial Tension of (Brines + CO_2): (0.864 NaCl + 0.136 KCl) at Temperatures between (298 and 448) K, Pressures between (2 and 50) MPa, and Total Molalities of (1 to 5) mol·kg-1, *Journal of Chemical & Engineering Data*, 57(4), 1078-1088, doi: 10.1021/je201062r.

[59] Arif, M., Al-Yaseri, A.Z., Barifcani, A., Lebedev, M., and S. Iglauer (2016) Impact of pressure and CO_2-brine interfacial tension: Implications for carbon geo-sequestration, *Journal of Colloid and Interface Science*, 462, 208-215.

[60] Armstrong, R.T., Porter, M.L., and D. Wildenschild (2012) Linking pore scale interfacial curvature to column-scale capillary pressure, *Advances in Water Resources*, 46, 55–62.